

Precipitation fronts and the reflection and transmission of tropical disturbances

Olivier Pauluis,^{a*} Dargan M. W. Frierson^b and Andrew J. Majda^a

^a *Courant Institute of Mathematical Sciences, New York University, USA*

^b *University of Washington, Seattle, USA*

ABSTRACT: This paper investigates the interactions between precipitation and the circulation in an idealized model for the tropical atmosphere where convection is represented by a quasi-equilibrium closure. When studying large-scale circulation in the Tropics, the governing equations can be further simplified by making the strict quasi-equilibrium assumption which considers that convection acts to instantaneously adjust the atmospheric temperature profile to a moist adiabatic lapse rate. It is shown here that, under this assumption, the interface between the precipitating and non-precipitating regions exhibits a discontinuity in the precipitation rate and vertical velocity. Furthermore, this interface, referred to as a precipitation front, moves at a velocity distinct from the propagation speed of dry and moist disturbances. The theory predicts the existence of three types of precipitation fronts: drying fronts, slow moistening fronts and fast moistening fronts. In previous studies, numerical simulations have demonstrated the existence of the three types of front, and have also confirmed that the precipitation front theory offers a good approximation for the behaviour of the interface between dry and moist regions for finite value of the convective adjustment time.

A new framework is proposed here in which the encounter of an atmospheric disturbance and the edge of a precipitation region is recast as a Riemann problem. It is shown that, for any precipitation fronts, there are three incident characteristics but only two outgoing characteristics. This makes it possible to solve simultaneously for the intensity of the outgoing invariants and the propagation speed of the front. This also implies that atmospheric disturbances will be partially transmitted and partially reflected when encountering a precipitation front. For small perturbations, linear reflection and transmission coefficients can be computed analytically. These results also indicate that disturbances can be amplified through over-transmission or over-reflection. These theoretical results are confirmed in numerical simulations of an idealized Walker circulation. A solution that includes a stationary precipitation front is perturbed by adding a small-amplitude gravity wave, convectively coupled gravity wave, or moisture disturbance. All numerical simulations exhibit reflection and transmission of the incoming signal, and one simulation shows a case of over-transmission of the incoming disturbance. Copyright © 2008 Royal Meteorological Society

KEY WORDS moist convection; quasi-equilibrium; atmospheric dynamics

Received 14 May 2007; Revised 3 March 2008; Accepted 17 March 2008

1. Introduction

The interaction between convection and the large-scale circulation is one of the central problems for our understanding of the tropical atmosphere. It is a key element in a wide variety of phenomena, ranging from the Hadley circulation (Satoh, 1994; Pauluis, 2004), Walker circulation (Bretherton and Sobel, 2002), intraseasonal variability (Madden–Julian Oscillation), hurricanes (Emanuel, 1986), or equatorial waves (Wheeler and Kiladis, 1999). At the core of the interactions lie two fundamental properties of moist air. First, as a parcel of moist air ascends, its temperature decreases because of its adiabatic expansion. After a sufficient drop in temperature, the parcel becomes saturated and water vapour condenses. Hence, any sustained ascending motion in the tropical atmosphere is

associated with clouds and precipitation. Second, the condensation of water vapour results in a significant release of latent heat that compensates partially for the adiabatic cooling. This latent heat release modifies the temperature of the atmosphere, which in turn impacts on the circulation. The balance between these two feedbacks – the enhancement of precipitation in ascending regions, and the atmospheric response to latent heat release – has profound implications for the dynamics of the tropical regions.

Convective motions take place on horizontal scales of the order of 10 km that are much smaller than the synoptic and planetary scales (from 1000 to 10 000 km). The large-scale separation has prevented until recently explicit numerical simulations that would resolve both the convective and planetary scales. General-circulation models (GCMs), which are designed to study the planetary and synoptic-scale circulation, have a horizontal resolution of the order of 100 km, which is insufficient

* Correspondence to: Olivier Pauluis, Courant Institute of Mathematical Sciences, 251 Mercer Street, New York, NY 10012, USA.
E-mail: pauluis@cims.nyu.edu

to adequately resolve convective motions (Satoh *et al.*, 2005). Instead, GCMs rely on cumulus parametrizations that determine the behaviour of convective systems based on semi-empirical closure assumptions. One of the most widely used convective closures is the quasi-equilibrium theory originally proposed by Arakawa and Schubert (1974). This closure is at the core of other representations of convection such as that of Betts and Miller (Betts, 1986; Betts and Miller, 1986), or Emanuel (1991). The quasi-equilibrium theory postulates that convective motions act to eliminate convective instability over a convective adjustment time of a few hours. As a result, a convective region is in a state of quasi-equilibrium between the destabilizing effects of the large-scale circulation and external heat sources and the stabilization by convective motions. As the convective adjustment time is short in comparison to the time-scale associated with synoptic or planetary circulation, the amount of convective instability, quantified in terms of the cloud work function (Arakawa and Schubert, 1974) or Convective Available Potential Energy (CAPE; Xu and Emanuel, 1989) remains small in convectively active regions.

The quasi-equilibrium theory predicts that the interaction of convection and large-scale circulation should result in the existence of convectively coupled gravity waves (Neelin *et al.*, 1987; Emanuel, 1987; Emanuel *et al.*, 1994 – ENB below). In the quasi-equilibrium framework, convection is more intense during periods of large-scale ascent, so that latent heat release due to condensation compensates partially for the adiabatic cooling. As a result of this correlation between latent heat release and ascent, the propagation speed of a disturbance is reduced in comparison to what it would be in the absence of condensation. Wheeler and Kiladis (1999) identify convectively coupled equatorial waves as well as their faster uncoupled counterparts in satellite observations. They estimate that convectively coupled waves propagate horizontally at a speed of about 15 m s^{-1} , which is about three times slower than a dry wave with the same depth.

Deep convection is not active over the entire tropical atmosphere. Rather, one expects to find ‘moist’ regions of active precipitation, and ‘dry’ regions with little or no precipitation. In agreement with the quasi-equilibrium theory, one expects disturbances in moist regions to move at a slower speed than in dry regions. This brings to mind an analogy with optics in which the speed of light is affected by the materials through which it propagates. In particular, a sudden change in propagation speed at the boundary between two different materials results in partial reflection and transmission of an incident wave. As it will be shown in this paper, a similar behaviour occurs when an atmospheric disturbance moves between dry and moist regions.

A key distinction between optics and atmospheric dynamics is that the location of the boundary between the dry and moist regions is not at a fixed location, but depends on the atmospheric state itself. In order to determine the reflection and transmission of an atmospheric

disturbance between dry and moist regions, one must also predict how the interface is affected by such disturbance, i.e. how the moist and dry regions move. One approach to this problem is to investigate the physical processes associated with the onset of precipitation and with the transition between different convective regimes such as shallow convection, congestus and deep convection. This is a very complex issue involving cloud microphysics, thermodynamics and turbulence among other sub-fields of atmospheric sciences, but this is not the focus of this paper. Rather, we are interested here in understanding the dynamical impacts of such a transition between precipitating and non-precipitating regimes. We will do this in the context of a very idealized framework based on the Strict Quasi-Equilibrium (SQE) assumption proposed by ENB, combined with the precipitation fronts theory originally discussed in Fierson *et al.* (2004 – FMP below).

One of the key parameters in quasi-equilibrium closures is the convective adjustment time, i.e. the time it takes for convection to remove convective instability. Various studies argue that this time should be between 2 and 24 hours (Betts, 1986; Bretherton *et al.*, 2004). Given that this time-scale is much shorter than the time-scale of the planetary-scale circulation, ENB have proposed SQE as the limit of the quasi-equilibrium theory for infinitely short convective adjustment time. In SQE, the atmosphere is instantaneously relaxed toward a moist adiabatic temperature profile in convective regions corresponding to the boundary-layer entropy. Such a moist adiabatic temperature profile is associated with a specific vertical structure in the horizontal pressure gradient, and translates into particular velocity profiles. The interaction between circulation and convection then results in the existence of convectively coupled gravity waves described by ENB. As such, SQE offers an elegant simplifying assumption for theoretical investigations of the interactions of convection and the planetary scale.

However the SQE framework as presented in ENB has an important limitation: it can only be applied for an atmosphere where there is precipitation everywhere. The key issue here is to determine the behaviour of the interface between dry and moist regions. At the core of this problem lies the physical requirement that the precipitation rate P can only be positive:

$$P \geq 0. \quad (1)$$

This constraint imposes a strong nonlinearity on the flow; for any solution of the equations of motion which produces a given precipitation rate $P > 0$, the reverse circulation has a negative precipitation rate and is not realizable.

The mathematical treatment of the interface between dry and moist regions in SQE is addressed by the precipitation front theory proposed by FMP. A simplified discussion of the FMP theory is presented in section 2. This theory is based on an idealized model similar to the Quasi-equilibrium Tropical Circulation model (QTCM; Neelin and Zeng, 2000), with a quasi-equilibrium closure

for the precipitation rate. From a mathematical point of view, the key finding in FMP is that the quasi-equilibrium formulation for the precipitation is dissipative not only in term of the state variables, but also in terms of their first-order derivatives. In the limit of infinitely short adjustment time, dissipation is concentrated at the interface between the dry and moist regions. This interface, which is referred to in FMP as a precipitation front, exhibits discontinuities in the precipitation rate and vertical velocity, and in the horizontal temperature and humidity gradients. In most cases, precipitation fronts are not stationary, but move at a velocity distinct from the dry and moist propagation speeds, and can be separated into three categories: the drying fronts, the slow moistening fronts and the fast moistening fronts. Conceptually, the precipitation fronts theory discussed by FMP makes it possible to determine the evolution of the interface between the dry and moist regions under the SQE assumption.

In this paper, we investigate the interaction between a precipitation front and an incident disturbance. The problem envisaged here is the one-dimensional (1D) equivalent of an equatorial Kelvin or Rossby wave coming across the edge of a precipitating region, although a similar problem could arise under other circumstances. In section 3, the theory for precipitation fronts is recast in terms of a Riemann problem. The governing equations can be re-written in terms of Riemann invariants that are conserved along the corresponding characteristics. In the dry regions, there are three Riemann invariants, two of them corresponding to propagating gravity waves, and a third one corresponding to a moisture trace advected by the background flow. In the moist regions, there are only two invariants corresponding to coupled convective-gravity waves. Each type of precipitation front intercepts three different characteristics, while only two characteristics are radiating away from the front. It is shown that the front speed and the Riemann invariants on the two outgoing characteristics are uniquely determined by the invariants on the incident characteristics. It is also shown that precipitation fronts are associated with a nonlinear transmission and reflection of a signal incident on the fronts. In the case of a small perturbation, linear reflection and transmission coefficients can be determined analytically. These calculations indicates that the precipitation fronts can amplify a disturbance through over-reflection or over-transmission of an incoming signal. It is also shown that the encounter of a precipitation front and a humidity perturbation will generate gravity waves on both sides of the fronts.

In section 4, we present numerical simulations of the reflection and transmission of tropical disturbances at a precipitation front using the model of Khouider and Majda (2005a,b). Stationary precipitation fronts can be present at the edge of the moist regions in a Walker-like circulation in both one and two dimensions, as discussed in the Appendix. Three simulations show the interactions between a front and a dry gravity wave, between a front and a convectively coupled gravity wave, and between

a front and a moisture perturbation. These results are summarized in the last section, along with a discussion of the implications of the precipitation front theory for atmospheric dynamics.

2. Precipitation fronts

2.1. Model equations

The model used in FMP is based on a Galerkin truncation of the equations of motion into two vertical modes, an approach similar to the QTCM of Neelin and Zeng (2000). An equivalent set of equations can also be obtained for a two-layer model such as that of Lapeyre and Held (2004). For simplicity, the present discussion is limited to a 1D problem, but a complete treatment of a 2D precipitation front can be found in FMP. The zonal wind is given as the sum of the barotropic wind \bar{U} and first baroclinic mode U_1 :

$$U(x, z, t) = \bar{U} + U_1(x, t)\Psi_U(z),$$

with $\Psi_U(z) = \cos(z)$ the structure function for the wind. (z is a normalized depth that ranges from 0 at the surface to 1 at the tropopause.) In contrast with FMP, we will assume that barotropic wind \bar{U} is prescribed. The temperature and humidity are given by

$$T(x, z, t) = \bar{T}(z) + T_1(x, t)\Psi_T(z)$$

$$\text{and } Q(x, z, t) = \bar{Q}(z) + Q_1(x, t)\Psi_Q(z),$$

where $\bar{T}(z)$ and $\bar{Q}(z)$ are horizontally uniform temperature and humidity reference profiles, and $\Psi_T(z) = \sin(z)$ and $\Psi_Q(z) = 1$ are the structure functions for temperature and humidity. For simplicity, there is no external energy sources such as evaporation and radiative cooling in this section, although these will be included in section 4 in our examination of the steady Walker cell. The equations of motion, after FMP, are

$$\partial_t U_1 + \bar{U} \partial_x U_1 = \partial_x T_1, \quad (2a)$$

$$\partial_t T_1 + \bar{U} \partial_x T_1 = c_d^2 \partial_x U_1 + P, \quad (2b)$$

$$\partial_t Q_1 + \bar{U} \partial_x Q_1 = -c_d^2 \Delta \bar{Q} \partial_x U_1 - P. \quad (2c)$$

Here, the abbreviations ∂_t and ∂_x are used to denote the partial derivative with respect to time and the x direction. In the absence of precipitation (i.e. $P = 0$), the equations for baroclinic wind (2a) and temperature (2b) reduce to the shallow-water equations with a characteristic speed c_d . This dry propagation speed can be obtained from the Galerkin truncation. The procedure followed by FMP yields a value of

$$c_d^2 = \frac{1}{\pi} H C_p \partial_z \bar{T} + gH,$$

with H the depth of the atmosphere, and C_p the heat capacity at constant pressure. Typical values for the

Tropics would yield a propagation speed c_d between 40 and 50 m s⁻¹.

The moisture stratification $\Delta\bar{Q}$ is a function of the reference humidity profile \bar{Q} and structure function. A complete derivation of these equations is available in FMP, which is itself adapted from the procedure used in the QTCM (Neelin and Zeng, 2000). A key difference between the FMP model and the QTCM is that the humidity advection in our model is done solely by the barotropic wind. This results from the use of a uniform structure function in height for the humidity. In contrast, the QTCM includes a baroclinic advection term in the moisture equation. The potential consequences of such baroclinic moisture advection for the dynamics of the precipitation fronts are discussed in the final section.

The system of equations is incomplete until the precipitation rate P is specified. FMP consider a simple representation of deep convection in which precipitation relaxes the humidity perturbation to a reference value (in non-dimensional units) in regions where deep convection is active. In regions where convection is inactive, i.e. where the perturbation humidity is smaller than the critical value, the precipitation vanishes. This yields

$$P = \frac{Q_1 - Q_*}{\tau} \text{ for } Q_1 > Q_* \\ = 0 \text{ for } Q_1 \leq Q_*. \tag{3}$$

Here, τ is the convective relaxation time, and Q_* is the critical humidity at which convection is initiated. The critical humidity can be chosen to be a function of temperature ($Q_* = Q_s + \alpha T_1$), so that (3) can be viewed as relating the amount of precipitation to the amount of CAPE in the column. However, FMP show that, if a new humidity variable is defined by

$$Q'_1 = Q_1 - Q_s - \alpha T_1,$$

one obtains a new set of equations which is mathematically equivalent to the case $Q_* = 0$, so only this case is discussed hereafter. (From a physical point of view, the rescaled variable Q'_1 measures the convective instability in the column, and the humidity variable in the case $Q_* = 0$ should be interpreted as a substitute for CAPE.)

Formulation (3) for the precipitation rate corresponds to a Betts–Miller type of relaxation scheme. In the SQE limit, i.e. in the limit of vanishing τ , precipitation instantaneously relaxes the water content to its saturation value $Q_* = 0$ in the moist region. In this case, the precipitation must balance exactly the large-scale destabilization. In this case, we have

$$P = -c_d^2 \Delta\bar{Q} \partial_x U_1 \text{ for } Q_1 = 0 \text{ and } \partial_x U_1 < 0, \tag{4a}$$

$$P = 0 \text{ for } Q_1 < 0 \text{ or } \partial_x U_1 > 0. \tag{4b}$$

In the moist regions where (4a) applies, the temperature equation (2b) can then be written as

$$\partial_t T_1 + \bar{U} \partial_x T_1 = (1 - \Delta\bar{Q}) c_d^2 \partial_x U_1. \tag{5}$$

The moist regions in the SQE limit are governed by (2a) and (5) which correspond to the shallow-water equations with a moist propagation speed c_m that is smaller than the propagation speed in the dry region:

$$c_m = (1 - \Delta\bar{Q})^{1/2} c_d. \tag{6}$$

In our simplified model, $\Delta\bar{Q}$ is the ratio of the latent heat stratification to the dry static energy stratification. It depends on the structure functions for the vertical velocity and humidity and temperature. Yu *et al.* (1998) have shown that in the Tropics, the stratification for latent heat and dry static energy are closely balanced, which implies a value of $\Delta\bar{Q} \approx 0.9$. The corresponding moist speed is approximately $c_m \approx 0.3c_d \approx 15 \text{ m s}^{-1}$.

(2a)–(2c) reduce to the linear shallow-water equations, with different propagation speeds within the dry and moist regions. However, we have yet to describe how the boundary between the dry and moist regions itself evolves. This part of the problem is where the fundamental nonlinearity remains because the switch between precipitating $P > 0$ to non-precipitating $P = 0$ regimes is itself nonlinear. Before addressing the proper treatment for the interface between dry and moist regions in section 2.3, one must first ensure that the SQE limit is mathematically consistent when dry and moist regions are present.

2.2. Dissipation and smoothness of the solutions

In this section, we show that the solutions of (2a)–(3) are well-behaved in the SQE limit of infinitely short convective adjustment. Well-behaved here means that solutions are bounded and meet certain smoothness properties. The smoothness of the solution is the key element that will then be used to obtain the evolution of the interface between the dry and moist regions in section 2.3. From a physical point of view, a quantity that can be interpreted as a moist version of the available potential energy is found to be decreasing with time, implying that the SQE system is dissipative.

An equation for the sum of the available potential energy and kinetic energy can be obtained by multiplying (2a) by $c_d^2 U_1$ and (2b) by T_1 and adding them:

$$(\partial_t + \bar{U} \partial_x) \left(\frac{c_d^2 |U_1|^2}{2} + \frac{T_1^2}{2} \right) = \partial_x (c_d^2 U_1 T_1) + P T_1. \tag{7}$$

In the absence of precipitation ($P = 0$), the right-hand side is the divergence of a flux, and (7) corresponds to the global conservation of the sum of the available potential energy and kinetic energy in the shallow-water equations. However precipitation can act as a source or a sink of available potential energy depending on whether it is positively or negatively correlated with temperature. Hence, the sum of available and kinetic energy is not necessary conserved here.

It is nevertheless possible to add an additional component to the energy equation to account for the fluctuations of moisture. First, a saturation temperature is defined by

$$T_w = T_1 + \frac{Q_1}{\Delta \bar{Q}}.$$

Its tendency is obtained by combining (2b) and (2c):

$$\partial_t T_w + \bar{U} \partial_x T_w = -\frac{1 - \Delta \bar{Q}}{\Delta \bar{Q}} P \quad (8)$$

The saturation temperature can be thought of as the temperature that the atmosphere column would have if it were brought to saturation ($Q_1 = 0$) by imposing the necessary vertical motion in the column. (8) indicates that precipitation reduces the saturation temperature, which is otherwise unaffected by the circulation.

A moist available energy, ϵ , can then be defined as

$$\begin{aligned} \epsilon &= \frac{c_d^2 |U_1|^2}{2} + \frac{T_1^2}{2} + \frac{\Delta \bar{Q}}{1 - \Delta \bar{Q}} \frac{T_w^2}{2} \\ &= \frac{c_d^2 |U_1|^2}{2} + \frac{T_1^2}{2} + \frac{(\Delta \bar{Q} T_1 + Q_1)^2}{2 \Delta \bar{Q} (1 - \Delta \bar{Q})}. \end{aligned} \quad (9)$$

The tendency for ϵ is

$$\partial_t \epsilon + \bar{U} \partial_x \epsilon - \nabla \cdot (c_d^2 U_1 T) = -\frac{P Q_1}{\Delta \bar{Q}}. \quad (10)$$

In quasi-equilibrium, the precipitation is correlated with humidity (3), and the first term on the right hand-side is always negative:

$$\partial_t \epsilon - \nabla \cdot (c_d^2 U_1 T) \leq 0. \quad (11)$$

This indicates that the quasi-equilibrium system is a dissipative system. On a closed domain, the integral of ϵ can only decrease. As this integral is a quadratic norm, this guarantees that solutions remains bounded for all time. In SQE, the correlation between P and Q vanishes in the dry and moist regions. It may seem that the system becomes non-dissipative. However, as τ^{-1} becomes infinitely large, there is significant dissipation in a narrow region at the interface between the dry and moist regions.

Remarkably, the dissipative nature of the SQE system extends to the first-order derivatives of the state variable. We introduce the notation $W = -\partial_x U_1$, $T_x = \partial_x T_1$ and $Q_x = \partial_x Q_1$ for the gradients of the original state variables. A quantity ϵ_{grad} is defined by

$$\epsilon_{\text{grad}} = \frac{c_d^2 W^2 + c_d^2 T_x^2}{2} + \frac{(\Delta \bar{Q} T_x + Q_x)^2}{2 \Delta \bar{Q} (1 - \Delta \bar{Q})}. \quad (12)$$

Its tendency is given by

$$\partial_t \epsilon_{\text{grad}} + \bar{U} \partial_x \epsilon_{\text{grad}} + \partial_x (c_d^2 W T_x) = -\frac{Q_x \partial_x P}{\Delta \bar{Q}}. \quad (13)$$

As long as precipitation is a monotonically increasing function of humidity, i.e $dP/dQ_1 > 0$, the right-hand side of (13) is always negative:

$$-\frac{Q_x \partial_x P}{\Delta \bar{Q}} = -\frac{dP}{dQ_1} \frac{(Q_x)^2}{\Delta \bar{Q}} < 0. \quad (14)$$

Precipitation acts as a dissipative mechanism that reduces the global integral of ϵ_{grad} .

The fact that precipitation acts as a dissipative mechanism for both ϵ and ϵ_{grad} has important implications for the mathematical behavior of the solutions. The global integral of the sum of ϵ and ϵ_{grad} is a norm for the Sobolev space H_1 of functions with square integrable first derivatives. Such a space includes continuous functions which are piecewise differentiable, but excludes discontinuous functions. The dissipative nature of ϵ and ϵ_{grad} guarantees that if one starts with an initial condition belonging to the Sobolev space H_1 , it will remain there at all time. In particular, solutions with smooth initial conditions do not develop any discontinuities in U , T , or Q . This also ensures that solutions with discontinuities in their first-order derivatives are well-behaved and can be solved in the weak sense.

Higher-order derivatives do not exhibit the same dissipative properties. If one constructs an equivalent to ϵ based on the second derivatives, its tendency would include the term

$$-\partial_{xx} P \partial_{xx} Q = -\frac{dP}{dQ} (\partial_{xx} Q)^2 - \frac{d^2 P}{dQ^2} (\partial_x Q)^2 \partial_{xx} Q.$$

The second term on the right-hand side can be of either sign, and second-order derivatives can grow indefinitely on the convective time-scale. In the SQE limit of infinitely fast adjustment, this leads to an instantaneous generation of a discontinuity in the first derivatives of the state variables and in the precipitation rate. These discontinuities which develop at interfaces between dry and moist regions in the SQE limit are referred to as precipitation fronts.

2.3. Propagation of precipitation fronts

The governing equations can be rewritten in terms of the first-order derivatives $W = -\partial_x U_1$, $T_x = \partial_x T_1$ and $Q_x = \partial_x Q_1$, assuming no barotropic wind:

$$\partial_t W + \bar{U} \partial_x W = -\partial_x T_x, \quad (15a)$$

$$\partial_t T_x + \bar{U} \partial_x T_x = -c_d^2 \partial_x W + \partial_x P, \quad (15b)$$

$$\partial_t Q_x + \bar{U} \partial_x Q_x = \Delta \bar{Q} c_d^2 \partial_x W - \partial_x P. \quad (15c)$$

Discontinuities in W , T_x , or Q_x can be handled by using a weak formulation of the equations in which the governing equations (15a)–(15c) are integrated across the discontinuity. The fact that such solutions are mathematically well-behaved is guaranteed by the dissipation of the

quantities ϵ and ϵ_{grad} discussed in the previous section. Solutions are assumed to be of the form $(W, T_x, Q_x)(x - \{\bar{U} + s\}t)$, with the discontinuity located at $x - (\bar{U} + s)t = 0$, with s the displacement speed of the discontinuity respectively to the barotropic background wind. It is assumed here without loss of generality that the moist region is located on the positive side of the front. In practice, this means that, for an equation of the form

$$\partial_t \phi = \partial_x F(\phi),$$

integrating across a jump at $x = 0$ yields

$$-s[\phi] = [F(\phi)].$$

The bracket denotes a difference taken across the interface $[\phi] = \phi_+ - \phi_-$, and the indices $+$ and $-$ refer to the value of the function on the right and left side of the interface. The key assumption here is that the solution ϕ remains square integrable at all time. In the case of the moisture fronts, the dissipation of ϵ and ϵ_{grad} ((10) and (13)) guarantees that the solutions are well-defined. Applying this procedure to (15a)–(15c) yields the Rankine–Hugoniot conditions for this system:

$$-s[W] = -[T_x], \tag{16a}$$

$$-s[T_x] = -c_d^2[W] + [P], \tag{16b}$$

$$-s[Q_x] = c_d^2 \Delta \bar{Q}[W] - [P]. \tag{16c}$$

This is a system of three equations with nine unknowns. (4a)–(4b) yield the precipitation rates on both sides of the fronts:

$$P_+ = c_d^2 \Delta \bar{Q} W_+, \tag{17a}$$

$$P_- = 0. \tag{17b}$$

Using these in (16a) and (16b) gives the expression for the propagation speed of the front

$$s^2 = \frac{c_m^2 W_+ - c_d^2 W_-}{W_+ - W_-}. \tag{18}$$

However, not all solutions are valid. The solutions within the dry and moist regions must meet the constraints for the sign of both precipitation and humidity perturbation. Namely, on the moist side of the precipitation front, the precipitation must be positive, and the humidity is 0, i.e.

$$P_+ = c_d^2 \Delta \bar{Q} W_+ \geq 0, \tag{19a}$$

$$Q_{x+} = 0. \tag{19b}$$

Conversely, on the dry side, the precipitation vanishes, but the humidity must be negative:

$$P_- = 0, \tag{20a}$$

$$Q_{x-} = -\frac{1}{s} \Delta \bar{Q} W_- \geq 0. \tag{20b}$$

These constraints restrict the range of values s that can be realized. FMP identify three different sets of precipitation fronts: drying fronts, slow moistening fronts and fast moistening fronts. A drying front occurs when the interface moves into the moist region ($s > 0$), with

$$\text{Drying front: } W_+ > 0, W_- < 0, c_m < s < c_d. \tag{21}$$

Moistening fronts correspond to the interface moving into the dry region ($s < 0$). The propagation can either be faster than the dry speed in the case of a fast moistening front, with

$$\text{Fast moistening front: } W_- > W_+ > 0, s < -c_d, \tag{22}$$

(the negative front velocity here indicates a front propagating into the dry regions ($x < 0$)), or slower than the moist speed with

$$\text{Slow moistening front: } W_+ > W_- > 0, -c_m < s < 0. \tag{23}$$

The numerical experiments presented in FMP show that all three types of front are realizable and stable for small convective but finite adjustment time.

3. Precipitation fronts as a Riemann problem

The precipitation fronts found move at a speed that is distinct from the dry or moist speed. They intercept signals emanating from either the dry or moist regions, or both. The expression (10) cannot be used directly to predict the propagation speed of a front, as the vertical velocities on both sides of the front depend in part of the behaviour of the front itself. Instead, a self-consistent solution requires a recasting of the problem in terms of the Riemann invariants, and to determine the front speed from the values of the Riemann invariants on the characteristics incident on the front.

3.1. Characteristics in the moist and dry regions

The equations of motion (15a)–(15c) can be recast as the propagation of a set of Riemann invariants propagating along the corresponding characteristics. The problem here differs from the traditional Riemann problem that one encounters when studying the propagation of sound waves or shallow-water waves in that the Riemann invariants are different in the dry and the moist regions. In fact, due to the dissipative nature of the precipitation, it will be shown that there is one less Riemann invariant in the moist regions than in the dry regions.

In the dry regions, with $P = 0$, the three Riemann invariants are

$$A_{\text{dp}} = W + \frac{T_x}{c_d}, \tag{24a}$$

$$A_{\text{dn}} = W - \frac{T_x}{c_d}, \tag{24b}$$

$$A_{\text{dq}} = \Delta \bar{Q} T_x + Q_x. \tag{24c}$$

The equations can be rewritten as

$$\partial_t(A_{dn}) + (\bar{U} - c_d)\partial_x A_{dn} = 0, \tag{25a}$$

$$\partial_t(A_{dp}) + (\bar{U} + c_d)\partial_x A_{dp} = 0, \tag{25b}$$

$$\partial_t(A_{dq}) + \bar{U}\partial_x A_{dq} = 0. \tag{25c}$$

The three invariants propagate on three characteristics. The first two correspond to eastward- and westward-propagating gravity waves. The third invariant is the derivative of the quantity T_w introduced in section 2. It can be thought of as a moisture trace that retains information on the initial moisture distribution and is advected by the mean barotropic wind.

In the moist regions, precipitation enforces the humidity to be 0, and the system has one less one degree of freedom. It can be described by two Riemann invariants

$$A_{mp} = W + \frac{T_x}{c_m}, \tag{26a}$$

$$A_{mn} = W - \frac{T_x}{c_m}. \tag{26b}$$

The governing equations then become

$$\partial_t A_{mn} + (\bar{U} - c_m)\partial_x A_{mn} = 0, \tag{27a}$$

$$\partial_t A_{mp} + (\bar{U} + c_m)\partial_x A_{mp} = 0, \tag{27b}$$

$$Q_x = 0. \tag{27c}$$

These equations describe westward- and eastward-propagating waves moving at a speed c_m .

The evolution of the flow for a given set of initial conditions can be determined by the method of characteristics. For an atmosphere that is uniformly dry or moist, it is straightforward to determine the flow at any time by using conservation of Riemann invariants along the different characteristics. In the presence of a precipitation front however, one must also determine the propagation speed and the value of the characteristics coming out of the front from the knowledge of the incident characteristics. Each of the three types of precipitation fronts described in section 2 has three incident characteristics for only two ongoing ones. This makes it possible to solve the jump conditions (16a)–(16c) to obtain the front speed and outgoing characteristics from the knowledge of the incident characteristics for each type of front.

3.2. Drying front

A dry front propagates into the moist region at a speed (relative to the ambient barotropic wind) between the dry and moist speeds, as illustrated in Figure 1. There are three incident characteristics: the two moist characteristics A_{mp} and A_{mn} , and the incident dry characteristic A_{dp} that catches up with the front from the dry side. From these, we need to determine the propagation speed of the front s , and the values of the two characteristics A_{dn} and

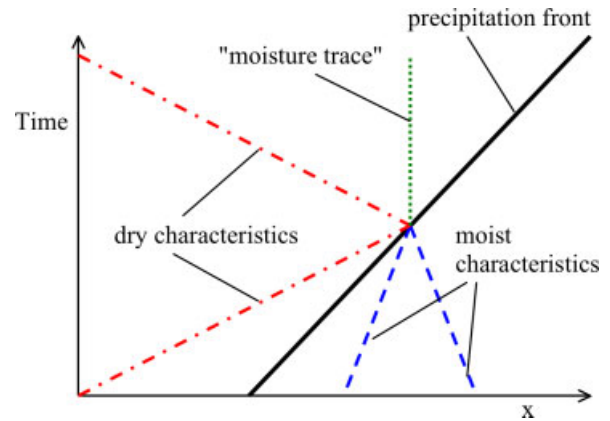


Figure 1. Schematic representation of the characteristics interacting with a propagating dry front. The front is propagating into the moist region, at a speed that is intermediate between that of the dry and moist characteristics. The moisture trace corresponds to the third characteristic in the dry region associated with the fluctuations of water vapour. This figure is available in colour online at www.interscience.wiley.com/qj

A_{dm} that emanate from the front. This can be done by solving the system of equations (16a)–(16c), yielding

$$s = \frac{2A_{dp} + c_m(1 - c_m^2)A_{mn} - c_m(1 + c_m^2)A_{mp}}{2A_{dp} - (1 - c_m)A_{mn} - (1 + c_m)A_{mp}}, \tag{28a}$$

$$A_{dn} = \frac{A_{dp}A_{mp}(1 - c_m)^2 + A_{dp}A_{mn}(1 + c_m)^2 - 4A_{mp}A_{mn}c_m^2}{4A_{dp} - A_{mn}(1 - c_m)^2 - A_{mp}(1 + c_m)^2}, \tag{28b}$$

$$A_{dq} = c_m(1 - c_m^2) \times \frac{(1 + c_m)A_{dp}A_{mn} - (1 - c_m)A_{dp}A_{mp} - 2c_mA_{mn}A_{mp}}{-2A_{dp} - c_m(1 - c_m)A_{mn} + c_m(1 + c_m)A_{mp}}. \tag{28c}$$

The propagation speed s here is taken relative to the barotropic wind. It is a nonlinear function of the incident characteristics. Figure 2(a) shows the variation of the front speed as a function of the incident dry wave, for $c_d = 1$ and $A_{mp} = A_{mn} = 1.0$. For a weak incident dry wave with $A_{dp} \approx c_m A_{mn}$, the fronts move at a low speed, with $s \approx c_m$ to c_d . For a stronger dry incident wave with $A_{dp} \gg A_{mn}$, the front speed becomes close to the dry propagation speed c_d . Figure 2(b) shows the amplitude of the dry gravity wave emanating from the same front.

3.3. Slow moistening front

The slow moistening front propagates into the dry region at a speed between 0 and the moist speed, as illustrated in Figure 3. The slow moistening front intersects three characteristics: the dry and moist characteristics A_{dp} and A_{mn} , and the stationary moisture trace A_{dq} . The propagation speed s and the Riemann invariants on the two emanating characteristics A_{dn} and A_{mp} are obtained by solving (16a)–(16c):

$$s = -\frac{(c_m - c_m^2) [A_{dp} + c_m A_{mn}]}{A_{dq} + (c_m - c_m^2)(A_{mn} - A_{dp})} \quad (29a)$$

$$A_{dn} = \frac{A_{dp}(c_m - 1) [A_{dq} + c_m(1 + c_m)^2 A_{mn}] + 2c_m^2 A_{dq} A_{mn}}{(1 + c_m)A_{dq} + (c_m - c_m^3)[(1 - c_m)A_{mn} - 2A_{dp}]} \quad (29b)$$

$$A_{mp} = \frac{A_{mn}(c_m - c_m^2) [A_{dp}(1 + c_m)^2 + A_{dq}] + 2A_{dp}A_{dq}}{(c_m + c_m^2) [A_{dq} + A_{dp}(1 - c_m)^2 + 2A_{mn}(c_m - c_m^2)]} \quad (29c)$$

Figure 4 shows the propagation speed of a slow moistening front as a function of the amplitude of the dry incident wave. When the incident dry and moist invariants are comparable with $A_{dp} \approx c_m A_{mn}$, the front speed is close to zero. The front speed increases to c_m as the ratio A_{mn}/A_{dp} increases.

3.4. Fast moistening front

The slow moistening front propagates into the dry region at a speed faster than the dry speed, as illustrated in Figure 5. The fast moistening front intersects all three characteristics in the dry regions: both gravity wave characteristics A_{dp} and A_{dn} , and the stationary moisture trace A_{dq} . The propagation speed s and the two outgoing invariants are obtained by following the same procedure as before:

invariants (28a)–(30c) are nonlinear functions of the incoming invariants. Nevertheless, some insights can be gained by examining the linear problem that arises when considering the propagation of a small perturbation superimposed on a background flow.

From the point of view of linear wave theory, the moist and dry regions are characterized by two different refraction indices. The abrupt transition in the refraction index that occurs at the precipitation front results in partial refraction and partial transition of an incident wave. Suppose that the initial conditions are given by specifying the invariants $A_{in,l}(x)$, $l = 1, 2, 3$ on the three incident characteristics at time 0. The location of the front $x_F(t)$ must here obey $dx_F/dt = s$, since the front speed obtained s from the value of the characteristics given by (28a), (29a) or (30a). Furthermore, the value of the invariant $A_{out,k}(t)$, $k = 1, 2$ on the two characteristics

$$s = -\frac{(1 - c_m^2) (A_{dp} + A_{dn})}{c_m^2 (A_{dn} - A_{dq}) - A_{dn} + A_{dp} - 2A_{dq}} \quad (30a)$$

$$A_{mp} = \frac{A_{dn}(1 - c_m) [A_{dq} + 2A_{dp}(c_m^2 + c_m)] + A_{dp}A_{dq}(c_m + 1)}{(c_m - c_m^3) [A_{dp}(1 - c_m) + A_{dn}(1 + c_m)] + 2A_{dq}c_m^2} \quad (30b)$$

$$A_{mn} = \frac{A_{dn}[2A_{dp}(c_m - c_m^3) - (1 + c_m)A_{dq}] - A_{dp}A_{dq}(1 - c_m)}{(c_m - c_m^3) [A_{dn}(1 - c_m) + A_{dp}(1 + c_m)] - 2A_{dq}c_m^2} \quad (30c)$$

A fast moistening front propagates faster than any characteristics. There is thus no information carried by the front itself. Rather than a propagating signal, one can think of such a front as being associated with the onset of precipitation over a wide area when the atmospheric column become convectively unstable.

3.5. Reflection and transmission

Precipitation fronts propagate at a speed that is distinct from that of the characteristics in moist and dry regions. The front speed is such that they always intercept three characteristics, while only two characteristics emanate from the front. When either side of the front is perturbed, a signal will propagate on a characteristic incident to the front. When the perturbation reaches the front, it will affect both the motion of the front and the characteristics emanating from it. This is inherently a nonlinear problem, and indeed all the expressions for the various outgoing

emanating from the front at time t can also be determined from the incoming invariants, i.e.

$$A_{out,k}(t) = A_{out,k} [A_{in,1}\{x_F(t) - c_1 t\}, A_{in,2}\{x_F(t) - c_2 t\}, A_{in,3}\{x_F(t) - c_3 t\}]. \quad (31)$$

Here, the two functions $A_{out,k}$, for $k = 1, 2$ are given by (28b)–(28c), (29b)–(29c) or (30b)–(30c).

We can now separate the initial condition between an unperturbed condition $A_{in,l}^0(x)$ and a small disturbance $A_{in,l}^1(x)$, i.e

$$A_{in,l}(x) = A_{in,l}^0(x) + \delta A_{in,l}^1(x) \text{ for } l = 1, 2, 3, \quad (32)$$

with δ an arbitrary small parameter. The invariants on the outgoing characteristics can be then expanded in terms of the δ parameter:

$$A_{out,k}(t) = A_{out,k}^0(t) + \delta A_{out,k}^1(t) + o(\delta^2) \text{ for } k = 1, 2. \quad (33)$$

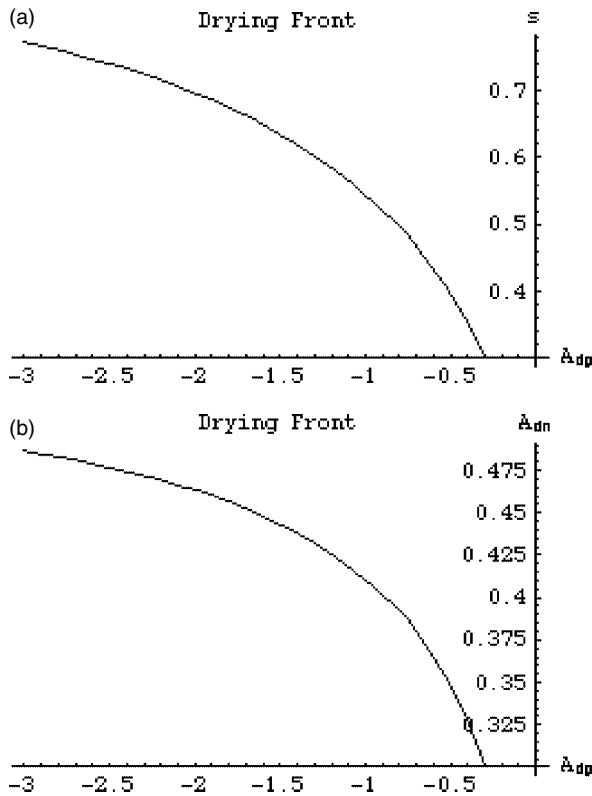


Figure 2. (a) Propagation speed, s , of a dry front as a function of the amplitude, A_{dp} , of the incident dry wave. (b) Amplitude, A_{dn} , of the dry wave generated by a dry front as a function of the amplitude, A_{dp} , of the incident dry wave. In both panels, $c_m = 0.3$, and $A_{mp} = A_{mn} = 1.0$.

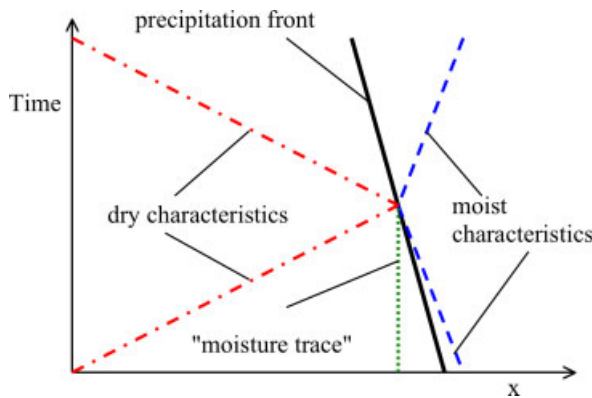


Figure 3. As Figure 1, but for the characteristics incident to a slow moist front propagating into the dry region at a speed lower than that of the moist characteristics. This figure is available in colour online at www.interscience.wiley.com/qj

The leading order term $A_{out,k}^0$ is the solution of the unperturbed problem. The linear response to a small perturbation $A_{in,k}^1$ can be obtained by expanding (31) in terms of δ . As long as the scale at which the unperturbed condition varies is much larger than the scale of perturbations, we can neglect the effects of the small variations in the location of the front $x_F(t)$. In this case, the linear response is

$$A_{out,k}^1 = \sum_{l=1}^3 \frac{\partial A_{out,k}}{\partial A_{in,l}} A_{in,l}^1 \{x_F(t) - c_l t\}. \quad (34)$$

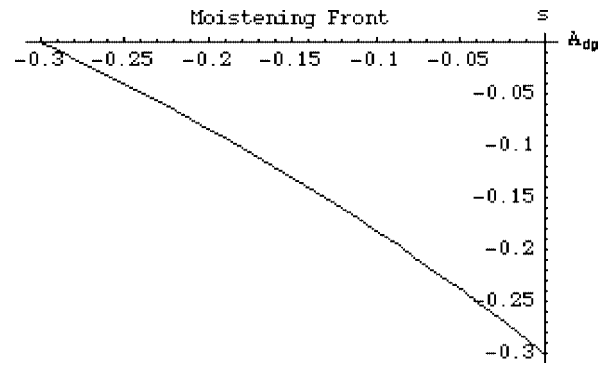


Figure 4. Propagation speed, s , of a moist front as a function of the amplitude, A_{dp} , of the incident dry wave, for $c_m = 0.3$, $A_{mn} = 1$ and $A_{dq} = 0$.

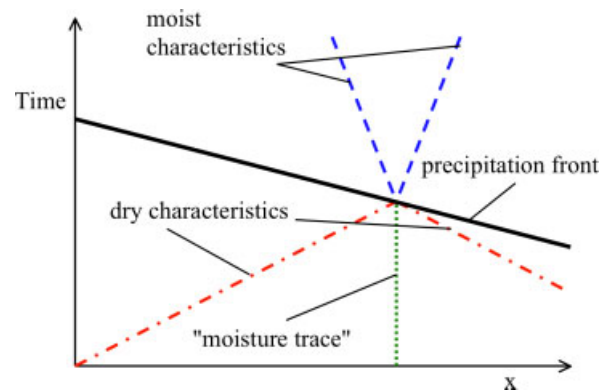


Figure 5. As Figure 1, but for the characteristics incident to a fast moist front propagating into the dry region at a speed lower than that of the moist characteristics. This figure is available in colour online at www.interscience.wiley.com/qj

The partial derivatives of (28b)–(28c), (29b)–(29c) or (30b)–(30c) correspond to the reflection and transmission coefficients for a small incident perturbations. For example, the reflection coefficient for an incident dry wave on a dry front is given by

$$R = \left. \frac{\partial A_{dn}}{\partial A_{dp}} \right|_{A_{mp}, A_{mn}}. \quad (35)$$

For any given front, we have a set of six different reflection–transmission coefficients given by the derivatives of the two outgoing amplitudes by the three incoming signals. These coefficients are not constant but depend on the incident characteristics. Figure 6 shows two of the reflection and transmission coefficients for a drying front as a function of the magnitude of the incident dry characteristic A_{dp} . In addition, as the different characteristics have different speeds relative to the front, the frequency and wavelength of the reflected/transmitted signals will be different.

In addition to the two propagating gravity waves, the dry region has a third characteristic: the moisture trace A_{dq} . This characteristic accounts for the fluctuation of the water vapor content in the moist region, and interacts directly with the different front. As illustrated in

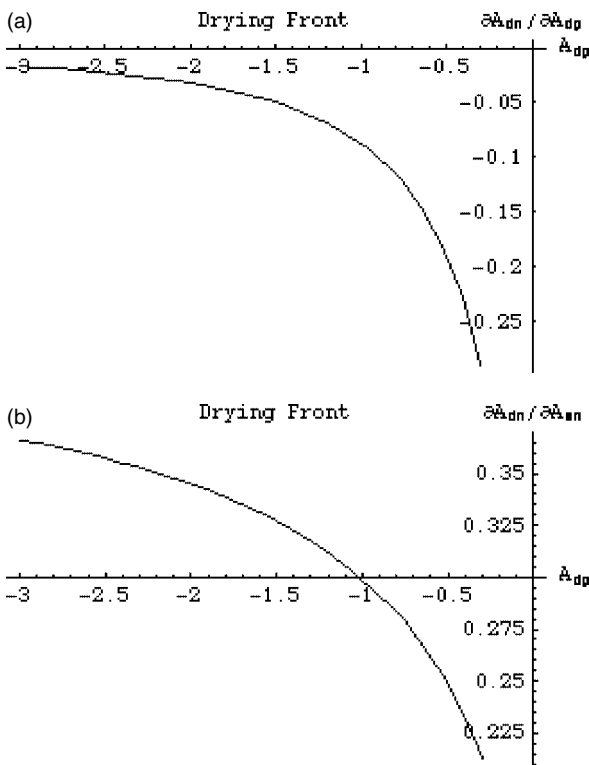


Figure 6. Reflection and transmission coefficients for a drying front as function of the amplitude, A_{dp} , of the incident dry wave, for $c_m = 0.3$, $A_{mn} = A_{mp} = 1$. (a) Reflection coefficient $\partial A_{dn}/\partial A_{dp}$ for an incident dry wave. (b) Transmission coefficient $\partial A_{dn}/\partial A_{mn}$ for a moist wave moving toward the dry region.

Figures 1 and 3, a moisture trace emanates from a drying front, and intercepts a moistening front. In particular, when a moistening front encounters a perturbation in the water vapor content, gravity waves will be generated in both the dry and moist regions. For a small amplitude perturbation, Figure 7 show the ‘reflection’ and ‘transmission’ coefficients for a moisture trace perturbation incident on moistening front. ‘Reflection’ here refers to the gravity wave emanating in the dry region – the same side as the the moisture trace – while ‘transmission’ refers to the gravity wave propagating on the moist side – opposite to the moisture trace.

Remarkably, precipitation fronts allow for both over-reflection and over-transmission of the incoming signal. Indeed, Figure 8(a) shows that the reflection coefficient for an incoming dry wave on a slow moist front can be larger than one. Similarly, Figure 8(b) indicates that the transmission coefficient for an incoming dry wave on the same slow moist front could be as large as 5. In both cases, fluctuations in the vertical velocity are amplified after encountering the precipitation front.

4. Interactions between a stationary front and a propagating disturbance

We will now illustrate the concepts discussed in the previous sections by looking at the interactions between a small disturbances and the edge of a moist region

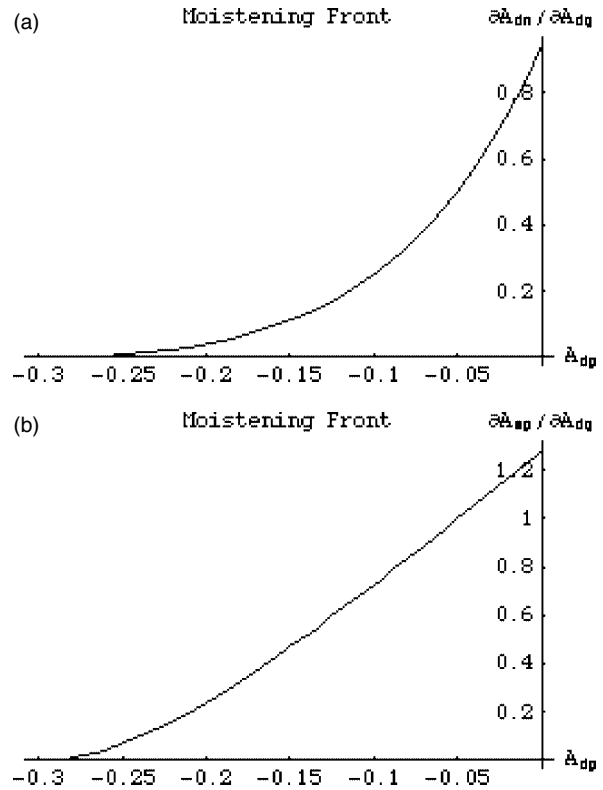


Figure 7. Reflection and transmission coefficient for the moisture trace incident to a moistening front for $c_m = 0.3$, $A_{mn} = 1$, and $A_{dq} = 0$, as a function of the amplitude, A_{dp} , of the incident dry wave: (a) ‘reflection’ coefficient $\partial A_{dn}/\partial A_{dq}$ for the gravity wave emanating in the dry region. (b) ‘transmission’ coefficient $\partial A_{mp}/\partial A_{dq}$ for the gravity wave emanating in the moist region.

of a Walker-like circulation. Precipitations can be made stationary through the advection of moisture. In the simple model used here, it is done by adding a uniform barotropic wind. Necessary conditions for the presence of a stationary precipitation front, as well as analytic solutions for idealized Walker circulations in one and two dimensions, are derived in the appendix.

The equations here are the same as (2a)–(2c) with additional terms for evaporation, radiation and damping:

$$\partial_t U_1 + \bar{U} \partial_x U_1 = \partial_x T - \frac{U_1}{\tau_D} \tag{36a}$$

$$\partial_t T + \bar{U} \partial_x T = c_d^2 \partial_x U_1 + P + \frac{T_{eq} - T}{\tau_D} \tag{36b}$$

$$\partial_t Q + \bar{U} \partial_x Q = -c_d^2 \Delta \bar{Q} \partial_x U_1 - P + \frac{Q_{eq} - Q}{\tau_D} \tag{36c}$$

Here, the damping time-scale τ_D is taken to be $\tau_D = 10$ days for all three variables. The equilibrium temperature T_{eq} and Q_{eq} can be any function of the location. Here, we will use

$$T_{eq} = 0, \tag{37a}$$

$$Q_{eq} = \sin\left(\frac{2\pi x}{L}\right), \tag{37b}$$

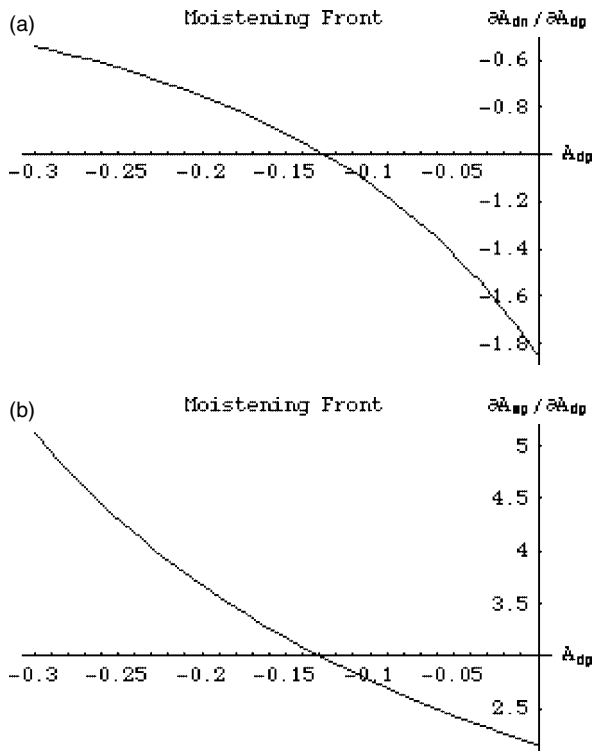


Figure 8. Reflection and transmission coefficients for a dry wave incident on a moistening front for $c_m = 0.3$, $A_{mn} = 1$, and $A_{dq} = 0$, as a function of the amplitude, A_{dp} , of the incident dry wave: (a) reflection coefficient $\partial A_{dn}/\partial A_{dp}$, and (b) transmission coefficient $\partial A_{mp}/\partial A_{dp}$.

with $L = 40\,000$ km the size of the domain. The barotropic wind is $\bar{U} = -0.1c_d = 5 \text{ m s}^{-1}$. The equations

are solved using the numerical model of Khouider and Majda (2005a,b) on a $40\,000$ km domain, with 4096 gridpoints. The convective adjustment time here is $\tau = 30$ minutes.

A stationary solution is obtained by integrating the solutions for 400 days. The results is shown in Figure 9. A moist region with large-scale ascent and heavy precipitation is located over the warm water. A stationary precipitation front is present on the eastern side of the moist region, with discontinuities in the precipitation rate P and in the partial derivatives of U , T , Q . In contrast, there is no such discontinuity on the western side of the precipitation region as the precipitation rate goes smoothly to 0. The solution is consistent with the theoretical prediction presented in the Appendix, and the stationary front can be interpreted as a slow moistening moving at a speed $s = -\bar{U}$ against the mean background flow.

A new initial condition is obtained by adding a small perturbation to the stationary solution. The initial perturbation is chosen so that it is localized in space and projects on a single Riemann invariant. The solution is then computed for 20–80 days. Because of the damping terms introduced in (36a)–(36c), all free-wave solutions from the original system (2a)–(2c) decay on a time-scale of $\tau_D = 10$ days. To compensate for this additional damping, the figures show the amplified perturbation

$$\phi'_a = \exp\left(\frac{t}{\tau_D}\right) \{\phi'(x, t) - \phi_0(x)\},$$

with ϕ' the perturbed solution, and ϕ_0 the stationary solution. We present here three experiments: a

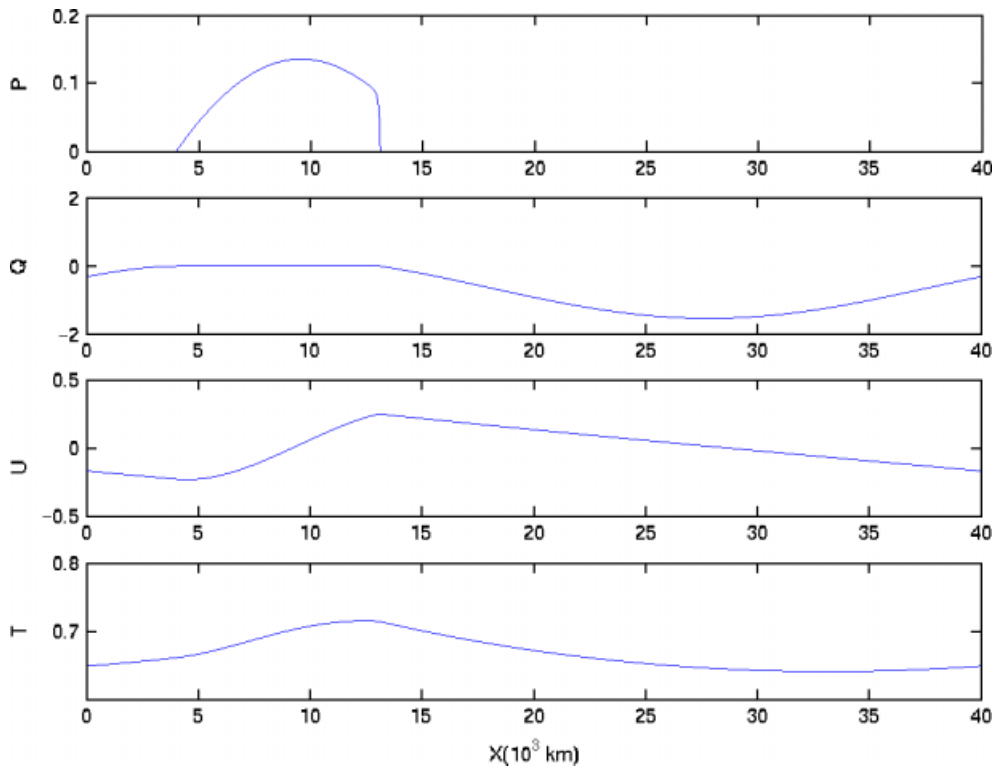


Figure 9. Stationary solution of the idealized Walker cell simulations. From the top: precipitation P , humidity Q_1 , horizontal wind U_1 , and temperature T_1 . This figure is available in colour online at www.interscience.wiley.com/qj

westward-moving disturbance initiated in the dry region, an eastward-moving disturbance starting in the moist region, and a moisture perturbation in the dry region.

The evolution of the westward-moving disturbance is shown on Figure 10, with the panel on the left showing the amplified zonal wind perturbation, and the panel on the right showing the amplified precipitation perturbation in the moist region (roughly for $4\,000\text{ km} < x < 13\,500\text{ km}$), and the humidity precipitation elsewhere. The disturbance moves westward until it encounters a precipitation front, at which point there is a sharp drop in the precipitation rate, followed by a period of enhanced precipitation. This succession of weaker then stronger precipitation at the front is due to the fact that the perturbation in zonal wind here is positive, and thus corresponds to downward velocity on its western side and upward velocity on its eastern side. After its initial encounter with the front, the disturbance has been split between a westward-moving convectively coupled gravity wave in the moist regions, and a reflected eastward-moving gravity wave in the dry regions.

In Figure 10, the maximum zonal wind perturbation occurs when the westward-propagating gravity wave

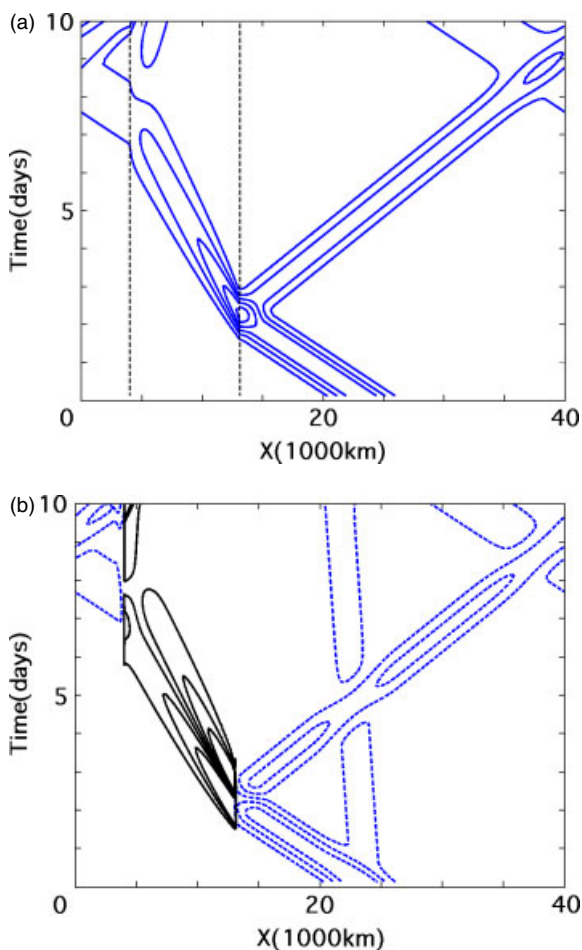


Figure 10. Time evolution of a westward-moving disturbance. (a) amplified zonal wind perturbation (solid) and edge of the precipitation regions (dashed). (b) amplified humidity perturbation (dashed) and amplified precipitation perturbation (solid). This figure is available in colour online at www.interscience.wiley.com/qj

encounters the precipitation front. This amplification is due to the over-transmission of the wave at the front. To confirm this, we show in Figure 11 the zonal wind perturbation before, during and after it encounters the front. The latter clearly exhibits the transmitted and reflected signal. As discussed in Emanuel (1993), the use of a finite value for the convective adjustment time results in a damping of the convectively coupled gravity waves. For small convective-adjustment time, the damping time-scale is proportional to $k^2\tau_c$, and is here close to 5 days. This damping is clearly evident in Figure 10. For comparison, Figure 11 compares the evolution of the same perturbation for convective adjustment time of 30 and 3 minutes. In the latter case, the transmitted signal is clearly larger than the incoming wave, and the maximum of the zonal wind is associated with the transmitted wave. It should be stressed that different variables are amplified differently. For instance, the vertical velocity perturbation is amplified by slightly more than a factor of 3 – due to fact that the horizontal scale of the disturbances is much shorter in the moist regions than in the dry regions – which is in good agreement with the value found in Figure 8.

Around day 8, the transmitted convectively coupled gravity-wave reaches the western edge of the moist regions, and so does the reflected gravity waves at around day 10. In both cases, we can observe gravity waves emanating in the dry and moist regions. In addition, there is a disturbance in the humidity field corresponding to the advection of the moisture trace by the barotropic wind. Such behaviour is not surprising if one views the transition between the dry and moist regions as an abrupt change in the refraction index. However, in the SQE limit, there are only two incident Riemann invariants for three outgoing characteristics, and the Riemann problem would be underdetermined at the interface. The theory discussed in section 3 cannot be used to quantitatively predict the behaviour of the disturbance at the western side of the moist regions. However, as the solution is smooth on the western edge the precipitation regions, it can be obtained by simply matching the state variables.

Figure 12 shows the evolution of an eastward-propagating convectively coupled gravity wave initiated in the moist region. The initial condition used here is slightly unbalanced which results in a weak westward-moving disturbance. Once the perturbation encounters the precipitation front, it splits between a transmitted dry gravity wave and a reflected moist gravity wave. In contrast to the dry gravity wave, the reflected and transmitted signals are weaker than in the incoming signal, though some of this should be attributed to the damping of the convectively coupled gravity waves. As in the case of the westward-propagating wave, one can observe a new set of waves generated when the disturbance later encounters the western side of the precipitation region.

Figure 13 shows the evolution of a disturbance of the moisture field. For the first 35 days, the perturbation

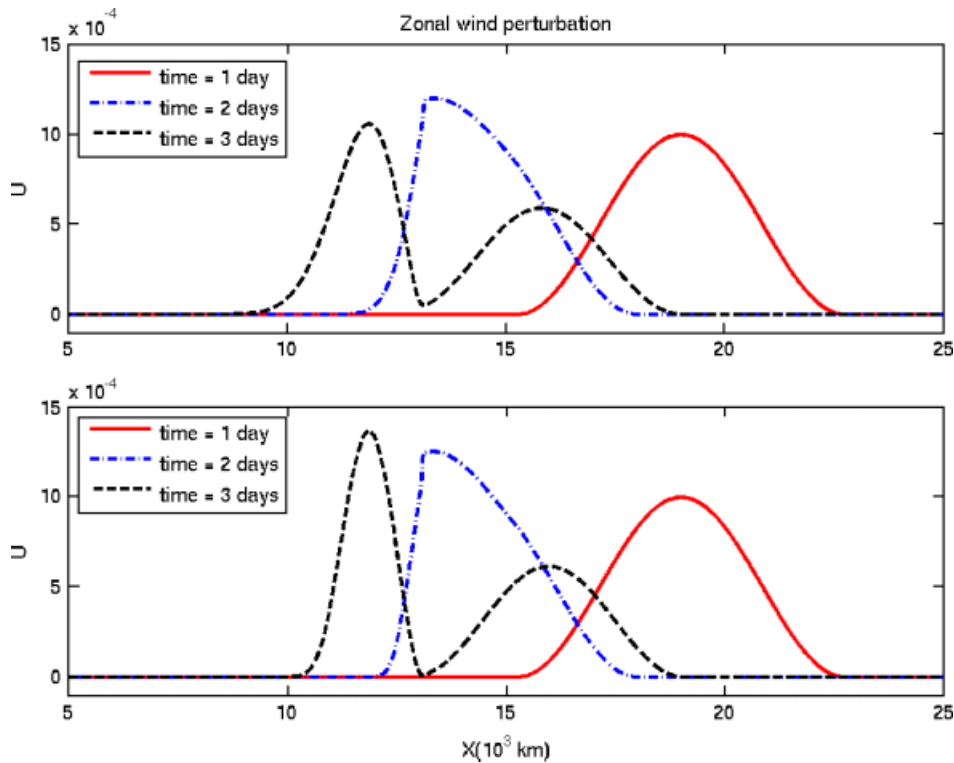


Figure 11. Zonal wind perturbation from the westward-propagating disturbance. (a) shows the solution for an adjustment time of 30 minutes, while (b) shows the same propagation for an adjustment time of 3 minutes. The solid line shows the disturbance before it encounters the front at time $t = 1$ day, the dash-dotted line shows the disturbance around the time it encounters the front at $t = 2$ days, and the dashed line shows the reflected and transmitted signal. The difference between the two panels is primarily due to the damping of convectively coupled gravity waves for finite convective adjustment time. This figure is available in colour online at www.interscience.wiley.com/qj

is slowly advected by the barotropic flow, and is only apparent in the humidity field. Upon its encounter with the precipitation front, the perturbation affects the precipitation rate, and generates a pair of gravity waves. The behaviour of the moisture perturbation also illustrates a particular issue for forecasting convection and tropical weather. Indeed, the moisture trace evolves very slowly on the advection time-scale. However it has no effect on the dynamics until it reaches a region of active convection, at which point its impact on the convection results in the generation of two gravity waves. This makes the assimilation of moisture particularly difficult, as moisture has its strongest impact at the interface between the dry and moist regions, but little effect elsewhere.

5. Discussion

In the limit of very short relaxation time, the quasi-equilibrium assumption results in solutions with a discontinuity in the precipitation field and the first derivatives of the state variables. These discontinuities, called precipitation fronts, occur at the interface between the dry and moist regions, and behave similarly to hydrodynamical shocks. Their propagation speeds can be obtained through a weak formulation of the equations of motions, and are distinct from the propagation speeds of the dry and moist characteristics of the system. Only specific

ranges for the values of the frontal speed are permitted, which led FMP to classify the fronts into three categories: the drying front, the fast moistening front and the slow moistening front. Combining the precipitation fronts theory of FMP with the SQE framework of Emanuel *et al.* (1994) offers a very simple conceptual framework to discuss the dynamics of the tropical atmosphere. In this framework, disturbances in dry and moist regions obey the linear shallow-water equations with different propagation speeds. The system however remains nonlinear due to the requirement that precipitation be always positive, which is captured by the nonlinear behaviour of the precipitation fronts. In this paper, we use this framework to analyze when an atmospheric disturbance moves between the precipitating and non-precipitating regions.

In section 3, we have recast the precipitation front theory in terms of the Riemann invariants, and shown how to obtain the propagation speed of the front as well as the values of the Riemann invariants emanating from the front. Disturbances encountering a precipitation front can be treated as moving between regions with different refractive indices. Hence, perturbations incident to a precipitation front will be partially reflected and partially transmitted across the front. Such reflection and transmission at the front is intrinsically a nonlinear problem. Nevertheless, a linear analysis confirms the reflection and refraction properties of the front, and indicates

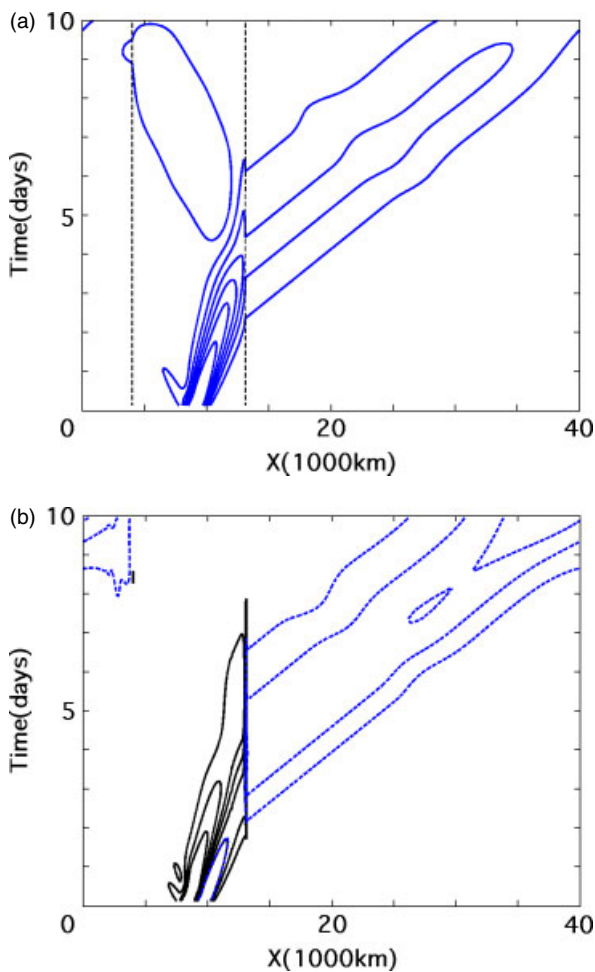


Figure 12. As Figure 10, but for an eastward-propagating disturbance. This figure is available in colour online at www.interscience.wiley.com/qj

that the amplitude of a disturbance can actually increase through over-reflection or over-transmission across the frontal boundary.

In section 4, we provided three examples of the transmission and reflections by looking at the interactions between a small perturbation and an idealized Walker-like circulation. We found significant amplification of an incoming dry gravity wave as it crosses a precipitation front. Interestingly, as at finite convective adjustment time, coupled convective gravity waves are damped; the amplification of gravity waves by a precipitation front results in the maximum wind perturbation occurring at the time when a disturbance encounters a precipitation front. The interaction between a precipitation front and a moisture perturbation also offers an example of how advection of moisture affects convection. A water vapour perturbation corresponds here to a perturbation in one of the three Riemann invariants – the moisture trace – in the dry regions, and is advected by the mean barotropic wind. Such a moisture perturbation has no effect on the dynamics, until it encounters a precipitation front, at which point it generates a pair of gravity waves. Conceptually, this illustrates the fact that, while moisture

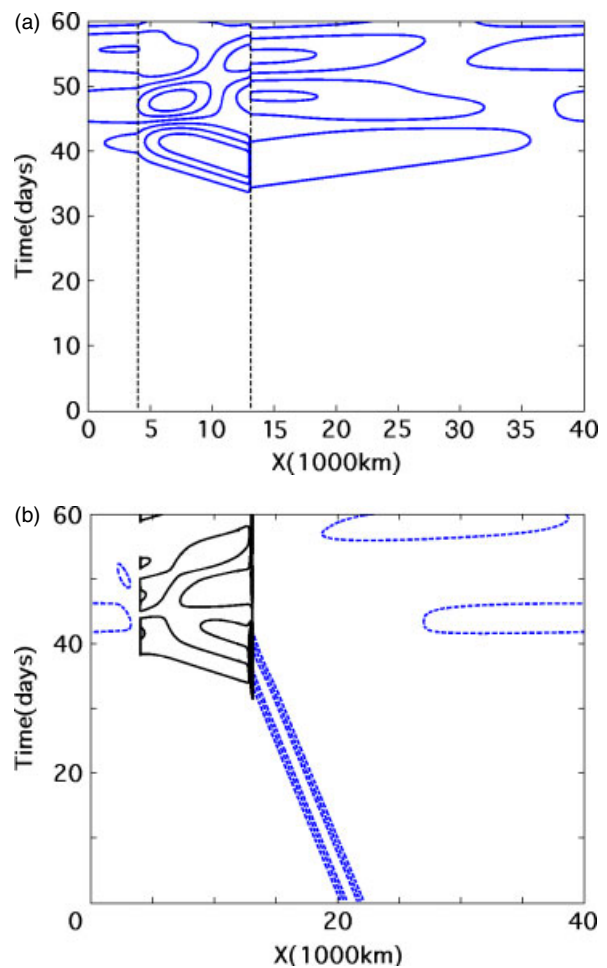


Figure 13. As Figure 10, but for a disturbance in the moisture field. Note the different time scale. This figure is available in colour online at www.interscience.wiley.com/qj

evolves on a relatively slow time-scale (at least in the dry regions) and could be used to improve long-term weather prediction, its impact on the dynamics is primarily concentrated in the transition zone between dry and moist regions.

An intriguing extension of the 1D theory discussed here is to investigate the propagation and reflection problem on an equatorial beta-plane. In this case, the linear solutions in the dry and moist regions would include Kelvin, Yanai and Rossby waves with the corresponding propagation speeds and Rossby radius. Solutions in the dry and moist regions would need to be matched at the interface between the dry and moist regions. The main difficulty is that the matching procedure must be performed along the entire interface, and not at a single location, as was the case in the 1D problem. The 2D Walker solution discussed in the Appendix is one example of such a solution where a stationary front is conveniently located along a longitude line. As for the 1D case, one does expect disturbances to partially propagate and transmit across the front. This implies for example that an incident Kelvin wave might be partially reflected as a Rossby wave when it moves from a moist to a dry region.

The mathematical framework for the precipitation fronts originally presented in FMP is based on a simplified version of the QTCM for which it is possible to fully derive the dissipation of a moist available energy. In contrast to the full QTCM, this model omits the advection of moisture by the baroclinic wind. Including such a term adds a quadratic nonlinearity and can induce new types of behaviour. A particular concern is that large-scale convergence can steepen the moisture gradient and generate a discontinuity in finite time. While such behaviour is a common consequence of advection and is unrelated to the convection, it makes it impossible to obtain a dissipation statement for the gradient formulation, as was done in section 2.3. The conditions that lead to an infinite increase in the humidity gradient are rather exceptional and not likely to correspond to an actual circulation. Furthermore, the weak solutions for the precipitation fronts should still hold as long as there is no discontinuity in the state variables. Hence, while the detailed effects of baroclinic moisture advection still need to be investigated, the existence and overall behaviour of the precipitation fronts should not be affected.

Even though the precipitation front theory only describes the onset of precipitation in the limit of infinitely short adjustment time, it also offers a good approximation for solutions within finite convective adjustment time. Frierson *et al.* (2004) find that the propagation speed of precipitation fronts in SQE also serves to predict the speed at which the interface between dry and moist regions moves for finite values of the adjustment time. Khouider and Majda (2005b) further confirm the existence of precipitation fronts in 1D and 2D numerical simulations. They also provide examples of nonlinear interactions between a precipitation front and an incident gravity wave. Stechmann and Majda (2006) show that for finite convective adjustment time, the frontal structure occupies a finite region, whose extent depends both on the frontal speed and the adjustment time. The frontal velocity and the far-field difference between dry and moist regions are however well captured by the SQE precipitation front theory. Simulations also show that other theoretical predictions of the precipitation fronts, such as the location of stationary fronts and the reflection/transmission of incident waves, also occur with finite relaxation time.

The physical interpretation of precipitation fronts also sheds some light on the original quasi-equilibrium theory. In their original argument, Arakawa and Schubert (1974) argue that convection acts to balance destabilization by large-scale atmospheric motions. However this adjustment is not instantaneous, and one thus expects that convection will be unbalanced for a short period or small region. In the idealized model used here, these adjustment regions are associated with the dissipation in the moist available potential energy (10) and its first derivative equivalent (13). The dissipative terms in these equations are associated with horizontal fluctuations of convective instability in the precipitation regions. In the limit of infinitely short adjustment time, the area

where this dissipation occurs collapses onto the frontal singularity. However, for finite adjustment times, there is a finite dissipative boundary layer at the interface between the dry and moist regions, as discussed in Stechmann and Majda (2006). This boundary layer corresponds to a zone where convective instability fluctuates, i.e. where convective adjustment cannot balance destabilization from external forcing. A key aspect of the precipitation front theory is that, while the boundary layer collapses in the limit of very short dissipation time, dissipation still takes place at the interface. In other words, right at the onset of precipitation, convection is unbalanced – even for infinitely short adjustment time.

One may question whether precipitation fronts correspond to an actual phenomenon, rather than an interesting conceptual model. While this issue cannot be answered at this point, it should be stressed here that the precipitation front theory offers a good approximation for the behaviour of the interface between the dry and moist regions for finite convective adjustment times. The precipitation fronts theory emphasizes the fact that the onset of precipitation introduces a very strong nonlinearity in the system resulting in very complex behaviour. Furthermore, given that many convection schemes used in GCMs are based on quasi-equilibrium concepts, the mathematical description of the precipitation fronts presented here can serve as a prototype to explain the behaviour of these more realistic models.

Acknowledgements

This work was supported by National Science Foundation grant ATM-0545047.

Appendix: Analytic solutions with stationary precipitation fronts

A stationary precipitation front can be made stationary by adding a mean barotropic wind \bar{U} to the governing equations. The existence of a stationary front depends on the magnitude of the barotropic wind, and is directly related to the propagation speed of the fronts discussed in section 2. In this appendix, we derive necessary conditions for the existence of a precipitation front, and use it to obtain the analytic solutions for an idealized Walker circulation in one and two dimensions.

A.1. Stationary precipitation fronts

We consider here the stationary solutions for prescribed evaporation, E , and radiation, R , rates. The equations of motion are

$$-\bar{U}W = \partial_x T, \quad (\text{A.1a})$$

$$\bar{U}\partial_x T = -c_d^2 W + P - R, \quad (\text{A.1b})$$

$$\bar{U}\partial_x Q = c_d^2 \Delta \bar{Q} W - P + E. \quad (\text{A.1c})$$

It is assumed here that the evaporation and radiation are smooth functions of x . The existence of steady solutions requires that the average radiation balances the average evaporation, i.e.

$$\int R dx = \int E dx. \tag{A.2}$$

In the absence of barotropic wind ($\bar{U} = 0$), (A.1a) implies that the temperature is uniform in a steady state solution $\partial_x T = 0$. Adding (A.1b) and (A.1c) also indicates that the vertical velocity W is as smooth as the radiation and evaporation. Hence, in the absence of barotropic flow, the stationary solution is as smooth as the forcing terms E and R , i.e. there is no stationary precipitation front.

In the presence of a barotropic flow ($\bar{U} \neq 0$), steady solutions can exhibit precipitation fronts, even when the radiation and evaporation fields are smooth. A necessary condition for the presence of a steady front is derived from (A.1a)–(A.1c). The precipitation rate can be obtained from (A.1a)–(A.1b):

$$P = R + (c_d^2 - \bar{U}^2)W. \tag{A.3}$$

As the precipitation vanishes in the dry region and the radiation is smooth, the precipitation on the moist side of the front P_m is given by

$$P_m = (c_d^2 - \bar{U}^2)(W_m - W_d), \tag{A.4}$$

where the subscripts d and m refer to values evaluated at the dry and moist sides of the boundary between dry and moist regions. Adding (A.1c) and (A.3) yields

$$(c_m^2 - \bar{U}^2)W = -\bar{U}\partial_x Q + E - R. \tag{A.5}$$

For smooth radiation and evaporation fields, using the fact that the humidity is uniform in the moist region ($\partial_x Q_m = 0$), we get

$$(c_m^2 - \bar{U}^2)(W_m - W_d) = \bar{U}\partial_x Q_d. \tag{A.6}$$

Eliminating $W_m - W_d$ between (A.4) and (A.6) yields

$$P_m = \frac{c_d^2 - \bar{U}^2}{c_m^2 - \bar{U}^2}(\bar{U}\partial_x Q_d). \tag{A.7}$$

For a given \bar{U} , the requirement that the precipitation be positive translates into a constraint on the sign of $\bar{U}\partial_x Q_d$. We refer here to upwind and downwind fronts depending on the position of the dry regions in relation to the frontal discontinuity. For an upwind front, the barotropic wind advects dry air into the frontal region. This situation is characterized by a negative correlation between the barotropic wind and water vapour gradient: $\bar{U}\partial_x Q_d > 0$. For a downwind front, this correlation is negative: $\bar{U}\partial_x Q_d < 0$. (A.7) then yields a necessary condition for the existence of precipitation fronts:

- (i) Upwind fronts can only exist for $|\bar{U}| \leq c_m$ or $|\bar{U}| > c_d$.
- (ii) Downwind fronts are present for $c_m < |\bar{U}| < c_d$.

These conditions are those necessary for the existence of a precipitation front traveling at the speed $s = -\bar{U}$.

A.2. Walker circulation in one dimension

We consider now a steady Walker solution on a periodic domain for a weak easterly barotropic wind $-c_m < \bar{U} < 0$. In this case, if a precipitation front is present, it should be on the eastern (upwind) side of the precipitating region, as the precipitation rate must vary smoothly on the western (downwind) side of the moist region. In the moist region, the solution of (A.1a)–(A.1c) is given by

$$\partial_x Q = 0, \tag{A.8a}$$

$$\partial_x T = -\bar{U}W, \tag{A.8b}$$

$$W = \frac{E - R}{c_m^2 - \bar{U}^2}, \tag{A.8c}$$

$$P = \frac{c_d^2 - \bar{U}^2}{c_m^2 - \bar{U}^2}E - \frac{c_d^2 - c_m^2}{c_m^2 - \bar{U}^2}R. \tag{A.8d}$$

If the precipitation rate (A.8d) is always positive, then the moist region extends through the entire domain in steady state.

When the precipitation rate given by (A.8d) is negative in some portion of the domain, there must be a dry (non-precipitating) region. In this region, the solution is given by

$$P = 0, \tag{A.9a}$$

$$\partial_x T = -\bar{U}W, \tag{A.9b}$$

$$W = \frac{-R}{c_d^2 - \bar{U}^2}, \tag{A.9c}$$

$$\partial_x Q = E - \frac{c_d^2 - c_m^2}{c_d^2 - \bar{U}^2}R. \tag{A.9d}$$

The issue here is to find the location of the interface between the dry and moist regions. Here, we take advantage of the fact that for our choice of the barotropic wind $-c_m < \bar{U} < 0$, only a downwind front can be present. This implies that the precipitation rate must be smooth on the western side of the moist region. The location x_w is chosen as one where the precipitation rate (A.8d) must vanish:

$$\frac{E(x_w)}{R(x_w)} - \frac{c_d^2 - c_m^2}{c_d^2 - \bar{U}^2} = 0. \tag{A.10}$$

For x_w to correspond to the western boundary of the precipitation regions, the precipitation rate must increase with x , i.e. $d(E/R)/dx > 0$. If (A.10) has only two roots, the location of the western boundary is uniquely

determined. (If there are more roots, some roots may not yield a valid solution, but at least one would. In this case, the proper solution would have to be found by trial and error on the different roots.) The moisture field in the dry region can be obtained by integrating (A.9d) westward:

$$Q(x) = Q_* - \int_x^{x_w} \left(E - \frac{c_d^2 - \bar{c}_m^2}{c_d^2 - \bar{U}^2} R \right) dx. \quad (\text{A.11})$$

The location of the eastern edge of the moist regions corresponds to the point x_E where the atmosphere becomes saturated again, i.e. where $Q(x_E) = 0$ in (A.11). Once x_E and x_W are found, the vertical velocity field can be determined directly, and the temperature field can be obtained by integrating (A.8b) and (A.9b). Figure 14

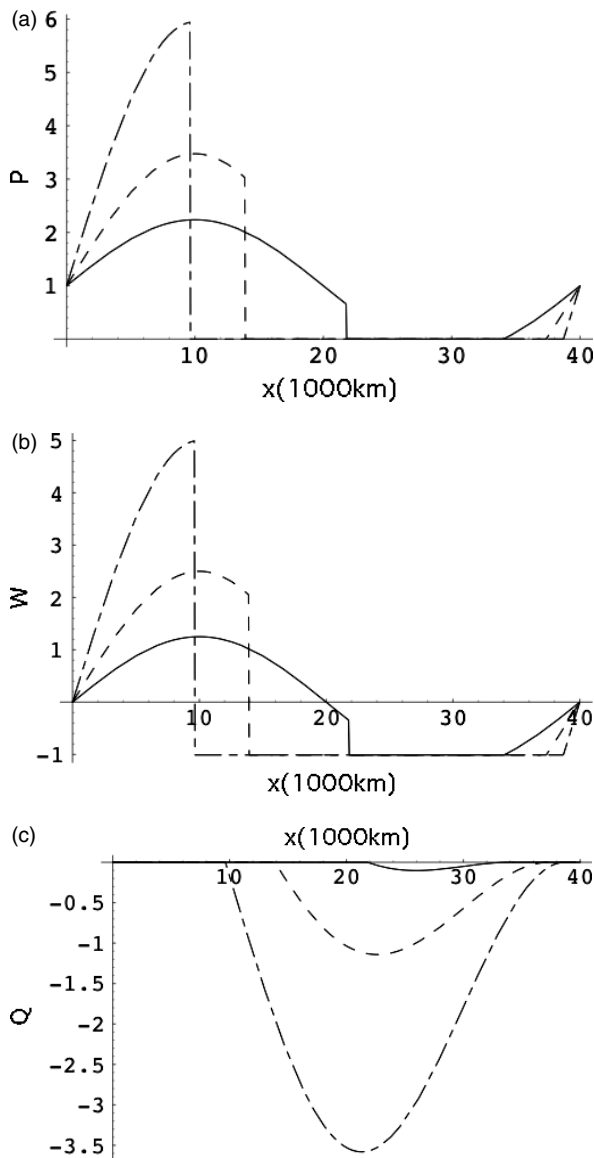


Figure 14. Solution for the 1D Walker circulation for $\bar{U} = -0.1c_d$ and with $E_0 = 0.1$ (solid line), $E_0 = 0.2$ (dashed line) and $E_0 = 0.4$ (dash-dotted line): (a) precipitation rate P , (b) vertical velocity W , and (c) humidity Q .

shows solutions for a forcing given by

$$R = 1, \quad (\text{A.12})$$

$$E = 1 + E_0 \sin\left(\frac{2\pi x}{L}\right). \quad (\text{A.13})$$

Here, $L = 40\,000$ km is the length of the domain. The values of c_d and c_m are 45 m s^{-1} and 15 m s^{-1} respectively. The two controlling parameters for this problem are \bar{U} and E_0 . Here, we use a mean wind of $\bar{U} = -0.1c_d$ (4.5 m s^{-1}) with E_0 values of 0.1, 0.2, and 0.4. All solutions exhibit a stationary precipitation front at the upwind side of the precipitation region, with discontinuities in the precipitation and vertical velocity. In contrast, the solution is smooth on the downwind side of the precipitation regions.

A.3. Walker circulation on an equatorial beta-plane.

On an equatorial beta-plane, the general solution would require a complete description of the frontal dynamics in two dimensions, and is beyond the scope of the present paper. Rather, solutions to the 2D Walker circulation problem are derived from 1D solutions, and are shown to exhibit fronts. Consider the equations of motion on an equatorial beta-plane for a steady flow:

$$\bar{U} \partial_x u_1 = \beta y v_1 + \partial_x T, \quad (\text{A.14a})$$

$$\bar{U} \partial_x v_1 = -\beta y u_1 + \partial_y T, \quad (\text{A.14b})$$

$$\bar{U} \partial_x T = c_d^2 (\partial_x u + \partial_y v) + P - R, \quad (\text{A.14c})$$

$$\bar{U} \partial_x Q = -\Delta \bar{Q} c_d^2 (\partial_x u + \partial_y v) - P + E. \quad (\text{A.14d})$$

Here, we consider only solutions that are decaying away from the Equator, with a structure function of the form $\exp(-\alpha y^2)$, with α an arbitrary function. The state variables as well as the evaporation and radiation fields are thus of the form:

$$u_1 = u_1(x) \exp(-\alpha y^2) \quad (\text{A.15a})$$

$$v_1 = 0 \quad (\text{A.15b})$$

$$T = T(x) \exp(-\alpha y^2) \quad (\text{A.15c})$$

$$Q = Q(x) \exp(-\alpha y^2) \quad (\text{A.15d})$$

$$R = R(x) \exp(-\alpha y^2) \quad (\text{A.15e})$$

$$E = E(x) \exp(-\alpha y^2) \quad (\text{A.15f})$$

The barotropic wind \bar{U} is imposed, and assumed to be constant everywhere. We are looking for a solution of equations (A.14a)–(A.14d) in which the meridional velocity v vanishes. In this case, the zonal wind equation (A.14a) is the same as for the 1D problem:

$$\bar{U} \partial_x u_1(x) = \partial_x T(x). \quad (\text{A.16})$$

The meridional momentum budget (A.14b) becomes

$$\beta y u_1(x) = -2\alpha y T(x). \quad (\text{A.17})$$

If the meridional structure of the solutions is such that

$$\alpha = -\frac{\beta}{2U}, \quad (\text{A.18})$$

and if there exists an x_0 such that

$$T(x_0) = u_1(x_0) = 0, \quad (\text{A.19})$$

then the equations for the zonal and meridional momentum (A.16) and (A.17) are equivalent. (A.18) imposes the meridional structure of the special solution of the Walker cell, while (A.19) can always be met, as the temperature in this problem is defined up to an additive constant. Under these conditions, the equations are exactly the same as the 1D Walker circulation equations, and the steady solutions to the 1D problem can be extended to specific solutions of the 2D Walker circulation. These special solutions are characterized by a purely zonal flow. For $-c_m < \bar{U} < 0$, these solutions can exhibit a stationary precipitation front at the eastern edge of the moist region.

References

- Arakawa A, Schubert WH. 1974. Interaction of a cumulus cloud ensemble with the large-scale environment, Part I. *J. Atmos. Sci.* **31**: 674–701.
- Betts AK. 1986. A new convective adjustment scheme. I: Observational and theoretical basis. *Q. J. R. Meteorol. Soc.* **112**: 677–692.
- Betts AK, Miller MJ. 1986. A new convective adjustment scheme. II: Single-column tests using GATE wave, BOMEX, and arctic air-mass datasets. *Q. J. R. Meteorol. Soc.* **112**: 693–709.
- Bretherton CS, Sobel AH. 2002. A simple model of a convectively coupled Walker circulation using the weak temperature gradient approximation. *J. Climate* **15**: 2907–2920.
- Bretherton CS, Peters ME, Back LE. 2004. Relationships between water vapor path and precipitation over the tropical oceans. *J. Climate* **17**: 1517–1528.
- Emanuel KA. 1986. An air-sea interaction theory for tropical cyclones. Part I: Steady maintenance. *J. Atmos. Sci.* **43**: 585–604.
- Emanuel KA. 1987. An air-sea interaction model of intraseasonal oscillations in the tropics. *J. Atmos. Sci.* **44**: 2324–2340.
- Emanuel KA. 1991. A scheme for representing cumulus convection in large-scale models. *J. Atmos. Sci.* **48**: 2313–2335.
- Emanuel KA. 1993. The effect of convective response time on WISHE modes. *J. Atmos. Sci.* **50**: 1763–1775.
- Emanuel KA, Neelin JD, Bretherton CS. 1994. On large-scale circulations in convecting atmospheres. *Q. J. R. Meteorol. Soc.* **120**: 1111–1143.
- Frierson DMW, Majda AJ, Pauluis O. 2004. Large scale dynamics of precipitation fronts in the tropical atmosphere: A novel relaxation limit. *Commun. Math. Sci.* **2**: 591–626.
- Khouider B, Majda AJ. 2005a. A non-oscillatory balanced scheme for an idealized tropical climate model. Part I: Algorithm and validation. *Theor. Comput. Fluid Dyn.* **19**: 331–354.
- Khouider B, Majda AJ. 2005b. A non-oscillatory balanced scheme for an idealized tropical climate model. Part II: Nonlinear coupling and moisture effects. *Theor. Comput. Fluid Dyn.* **19**: 355–375.
- Lapeyre G, Held IM. 2004. The role of moisture in the dynamics and energetics of turbulent baroclinic eddies. *J. Atmos. Sci.* **61**: 1693–1710.
- Neelin JD, Zeng N. 2000. A quasi-equilibrium tropical circulation model – Formulation. *J. Atmos. Sci.* **57**: 1741–1766.
- Neelin JD, Held IM, Cook KH. 1987. Evaporation-wind feedback and low-frequency variability in the tropical atmosphere. *J. Atmos. Sci.* **44**: 2341–2348.
- Pauluis O. 2004. Boundary layer dynamics and cross-equatorial Hadley circulation. *J. Atmos. Sci.* **61**: 1161–1173.
- Satoh M. 1994. Hadley circulations in radiative-convective equilibrium in an axially symmetric atmosphere. *J. Atmos. Sci.* **51**: 1947–1968.
- Satoh M, Tomita H, Miura H, Iga S, Nasuno T. 2005. Development of a global cloud resolving model of tropical convections a multi-scale structure of tropical convections. *J. Earth Simulator* **3**: 11–19.
- Stechmann SN, Majda AJ. 2006. The structure of precipitation fronts for finite relaxation time. *Theor. Comput. Fluid Dyn.* **20**: 377–404.
- Wheeler M, Kiladis GN. 1999. Convectively coupled equatorial waves: Analysis of clouds and temperature in the wavenumber-frequency domain. *J. Atmos. Sci.* **56**: 374–399.
- Xu K-M, Emanuel KA. 1989. Is the tropical atmosphere conditionally unstable? *Mon. Weather Rev.* **117**: 1471–1479.
- Yu JY, Chou C, Neelin JD. 1998. Estimating the gross moist stability of the tropical atmosphere. *J. Atmos. Sci.* **55**: 1354–1372.